Available online at www.sciencedirect.com
SCIENCE DIRECT®
Journal of Sound and Vibration 278 (2004) 461–477
JOURNAL OF SOUND AND VIBRATION
www.elsevier.com/locate/jsvi

Modal vibrations of a cylindrical radiator over an impedance plane

S.M. Hasheminejad*, M. Azarpeyvand

Department of Mechanical Engineering, Iran University of Science and Technology, Narmak, Tehran 16844, Iran

Received 20 November 2002; accepted 7 October 2003

Abstract

The problem of acoustic radiation from an infinite cylinder undergoing harmonic modal surface vibrations near a locally reacting planar boundary is considered. The formulation utilizes the appropriate wave field expansions, the classical method of images, and the translational addition theorem for cylindrical wave functions, along with a simple local surface reaction model involving a complex amplitude wave reflection coefficient applied to simulate the relevant boundary conditions for the given configuration. The analytical results are illustrated with a numerical example in which the cylindrical surface is immersed near a layer of fibrous material set on an impervious rigid wall. The numerical results reveal the important effects of interface local surface reaction and source position on the computed modal impedance component values and the radiated on-axis far-field pressure. The benchmark solution presented can lead to a better understanding of acoustic radiation from near-interface two-dimensional sources, which are commonly encountered problems in outdoor acoustics and noise control engineering. Eventually, it could be used to validate those found by numerical approximation techniques.

1. Introduction

There has been a developing interest in acoustics of fluid-saturated porous media due to its critical applications in various technical and engineering processes ranging from geophysics, atmospheric acoustics and ocean acoustics, to biophysics, architectural acoustics, and noise control engineering. In particular, there is an increasing demand to study propagation, attenuation and dispersion of elastic waves in granular media such as rock formations in petroleum reservoirs, ocean bed sedimentary layers, sound absorbing (impedance) ground and

*Corresponding author. Tel.: +98-21-73912936/+98-21-2557166; fax: +98-21-7451143.
E-mail address: hashemi@iust.ac.ir (S.M. Hasheminejad).

0022-460X/$ - see front matter © 2003 Elsevier Ltd. All rights reserved.
doi:10.1016/j.jsv.2003.10.039

also in fibrous medium such as biological tissues, polymer networks and sound absorbing materials.

One of the first elastic porous material models was that due to Beranek [1] who showed that two longitudinal waves can propagate through the flexible fibrous materials. Zwikker and Kosten [2] also found that two types of compressional waves can coexist in a porous material (i.e., the frame-borne wave and the airborne wave). Gassmann [3] presented the first concise model for harmonic plane wave propagation in an infinite fluid-saturated porous solid. His work is considered to be the first major breakthrough in predicting the elastic moduli of porous media at low frequencies. Gassmann's treatment, however, disregarded the relative viscous fluid/elastic solid motion that is known to be the main cause of energy loss in the high-frequency regime. Approaching the problem in a more unified manner, Biot [4–6] extended Gassman's work in statics to non-zero frequency and developed a straightforward and efficient two-phase theory for wave propagation, addressing such issues as wave speed, attenuation, dispersion and anisotropy. He formulated the appropriate constitutive equations and equations of motion in poroelastic media and predicted the existence of two types of dilatational (compressional) waves along with one rotational (shear) wave. For many years following the development of Biot theory of dynamic poroelasticity, the existence of Biot slow compressional (type II) wave remained the most controversial of its predictions within the seismology and underwater acoustics communities. Recently, the scientific groundwork for Biot's model is more firmly established through several experimental validations of its most fundamental predictions [7–9], leading to a renewed interest in the subject. Consequently, Biot's model has in time become the standard model for wave propagation in elastic porous media.

Many papers deal with absorption of a spherical wave by an absorbing plane. In particular, prediction of the sound field due to a simple point source in a homogenous medium above an impedance plane is a fundamentally important problem in many applications of outdoor acoustics and noise control engineering, which has been pursued by many authors [10–12]. In most of these studies, the aim has been to obtain simple near- and far-field approximations to describe the propagation of sound from the source above the impedance plane. On the other hand, the absorption of a cylindrical wave by an absorbing plane has found comparatively less attention, although a line source may be a good model for many practical source configurations. For example, rubber blocks hitting the ground generate a "line source" at the front edge of the tyre/road contact surface [13]. In this case the sound absorbing road surface is represented by an impedance boundary condition. Furthermore, the tyre and the road surface together form a horn-like geometry that leads to a substantial amplification of the radiated sound power (i.e., the so-called horn effect). Kropp et al. [14], applied a two-dimensional model based on a multipole synthesis to study this effect. They used a pair of (source-image) multipoles to fulfil the prescribed boundary conditions on the tyre and the road (impedance) surface simultaneously. In other applications the acoustic field due to a line source such as a traffic stream near sound absorbing traffic noise barriers and absorptive treatments to high rise building elements are investigated [15,16]. Habault and Filippi [17] analytically treated sound absorption of a cylindrical wave produced by a line source above an absorbing plane; they applied the method of solution that they have developed for the point source to the cylindrical wave absorption. Chandler-Wilde and Hothersall [18] discussed the more general case of an impedance strip in a plane of different impedance, and a monopole line source parallel to the strip. Rasmussen [19]

dealt with a line source over a locally reacting plane surface. He transformed the analysis by Chien and Soroka [20] from the problem of a point source to that of a line source. More recently, Mechel [21] presented a rigorous analysis for the sound field of a simple (monopole) line source above a plane absorber. He used saddle point integration to derive fast-computing approximations of the sound field.

Not all practical noise sources have monopolar characteristics, i.e., they are directional and do not behave as simple monopoles particularly at close range. In fact, there are many situations in which the multipole source strength is very large and there is no substantial contribution from monopole radiation (e.g., sound radiation from an oscillating sphere, rolling noise and aerodynamic jet noise). Under these circumstances, source description in terms of multipoles may be more useful [14,22–25]. On the other hand, the solutions of acoustic radiation problems involving a finite-sized source near a reacting (non-rigid) boundary seem to be quite sparse. The problem of radiation loading on a cylindrical (spherical) source freely suspended in a fluid-filled cylindrical (spherical) cavity embedded within a fluid-infiltrated elastic porous medium is tackled in Refs. [26,27]. Likewise, the more related problem of modal acoustic radiation impedance load on a spherical surface undergoing angularly periodic axisymmetric harmonic vibrations while immersed near the locally reacting planar boundary of an acoustic halfspace is examined in Ref. [28]. The principal objective of present work is to employ the theory of wave propagation in fluid-saturated porous materials to study acoustic radiation from a cylindrical surface undergoing harmonic modal vibrations near a homogeneous locally reacting planar interface. The solution of the problem is generated by systematically analyzing multi-scattering interaction between the vibrating cylinder and the impedance boundary that can be strong or weak depending on their separation, local surface reaction, and frequency.

2. Formulation

The problem geometry is illustrated in Fig. 1. The cylindrical surface is located above the locally reacting planar boundary of the acoustic halfspace, which is assumed to have a normalized admittance β. The method of images will be employed to efficiently take the presence of the wall into account [29]. The mirror image of the cylindrical surface lies at a distance $d/2$ below the interface. The problem can be analyzed by means of the standard methods of theoretical acoustics. The fluid present in the acoustic halfspace is assumed to be inviscid and ideal compressible that cannot support shear stresses making the state of stress in the fluid purely hydrostatic. Consequently, the time-harmonic field equations may conveniently be expressed in terms of a scalar velocity potential as [30]

$$\begin{aligned} \mathbf{u} &= -\nabla \Phi, \\ p &= -\mathrm{i}\omega\rho_0 \Phi, \\ \nabla^2 \Phi + k^2 \Phi &= 0, \end{aligned} \tag{1}$$

where $\mathbf{u}$ is the fluid-particle-velocity vector, p is the acoustic pressure in the fluid, and the complex wave number, $k(\omega)$, which is assumed to take the thermoviscous energy losses in the ambient fluid

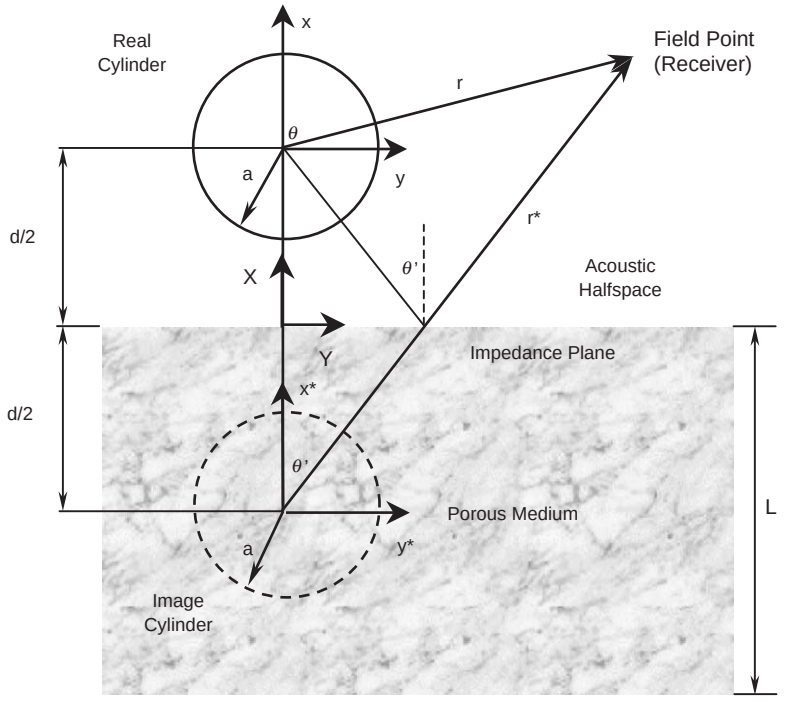

Fig. 1. Problem geometry.

(air) into account, is provided by the well-known approximate formula [30]

$$k(\omega) = \frac{\omega}{c_0}\left[1 + \mathrm{i}\frac{\omega\eta}{2\rho_0 c_0^2}\left(\frac{4}{3} + \frac{\eta_b}{\eta} + \frac{\gamma - 1}{Pr}\right)\right], \tag{2}$$

where c_0 is adiabatic speed of sound, η denotes shear viscosity, η_b is the bulk viscosity, ρ_0 and γ are density and specific heat ratio of the ambient fluid, Pr is the Prandtl number, and harmonic time variations have been assumed throughout with $\mathrm{e}^{-\mathrm{i}\omega t}$ dependence suppressed for simplicity.

The dynamics of the current multi-scattering problem may be expressed in terms of two scalar potentials: one corresponding to the waves disseminating from the real cylinder and the other relating to the waves from the image cylinder. Thus for z-independent motion in bi-cylindrical co-ordinates

$$\Phi_1(r, \theta, \omega) = \sum_{n=-\infty}^{\infty} a_n(\omega)\mathrm{H}_n(kr)\mathrm{e}^{\mathrm{i}n\theta},$$

$$\Phi_2(r^*, \theta^*, \omega) = \sum_{n=-\infty}^{\infty} b_n(\omega)\mathrm{H}_n(kr^*)\mathrm{e}^{\mathrm{i}n\theta^*}, \tag{3}$$

where $\mathrm{H}_n(\ )$ is the cylindrical Hankel function of the first kind and order n [31], and $a_n(\omega)$ and $b_n(\omega)$ are unknown modal coefficients.

In order to satisfy the appropriate boundary conditions the acoustic field contribution of the image (real) cylinder must be expressed with respect to the co-ordinate system of the real (image)

cylinder. Thus the classical translational addition theorem for bi-cylindrical co-ordinates [32] must be used:

$$\mathrm{H}_n(kr^*)\mathrm{e}^{\mathrm{i}n\theta^*} = \sum_{m=-\infty}^{\infty} \mathrm{J}_m(kr)\mathrm{H}_{n-m}(kd)\mathrm{e}^{\mathrm{i}m\theta},$$

$$\mathrm{H}_n(kr)\mathrm{e}^{\mathrm{i}n\theta} = \sum_{m=-\infty}^{\infty} \mathrm{J}_m(kr^*)\mathrm{H}_{m-n}(kd)\mathrm{e}^{\mathrm{i}m\theta^*}. \tag{4}$$

Next, to include the effect of halfspace boundary impedance on the radiation loading of the cylindrical source, the lucid theoretical development presented in Section 7.4 of the classical monograph by Morse and Ingard [29] is followed (see also Ref. [14]). Adopting similar arguments and incorporating the addition theorem (4) in the field expansions (3) allows the total potential field in the co-ordinate system of each cylinder to be expressed as

$$\begin{aligned}\Phi(r,\theta,\omega) &= \Phi_1(r,\theta,\omega) + R\Phi_2(r^*,\theta^*,\omega)\\ &= \sum_{n=-\infty}^{\infty} a_n(\omega)\mathrm{H}_n(kr)\mathrm{e}^{\mathrm{i}n\theta} + R\sum_{n=-\infty}^{\infty}\left(\sum_{m=-\infty}^{\infty}\mathrm{H}_{n-m}(kd)b_m(\omega)\right)\mathrm{J}_n(kr)\mathrm{e}^{\mathrm{i}n\theta}\end{aligned} \tag{5}$$

and

$$\begin{aligned}\Phi(r^*,\theta^*,\omega) &= R\Phi_1(r,\theta,\omega) + \Phi_2(r^*,\theta^*,\omega)\\ &= R\sum_{n=-\infty}^{\infty}\left(\sum_{m=-\infty}^{\infty}\mathrm{H}_{m-n}(kd)a_m(\omega)\right)\mathrm{J}_n(kr^*)\mathrm{e}^{\mathrm{i}n\theta^*} + \sum_{n=-\infty}^{\infty} b_n(\omega)\mathrm{H}_n(kr^*)\mathrm{e}^{\mathrm{i}n\theta^*},\end{aligned} \tag{6}$$

where the complex amplitude plane wave reflection coefficient, R, for the case when the field point is near the real cylinder's surface and the cylindrical surface is not located very close to the impedance boundary (Fig. 1), is approximated by [28]

$$R \approx \frac{1-\beta(\omega)}{1+\beta(\omega)}, \tag{7}$$

where $\beta(\omega) = \rho_0 c_0/Z_N(\omega)$ is the relative normal admittance of the locally reacting boundary, in which the surface normal impedance, $Z_N(\omega)$, can be readily determined by the expression [28]

$$Z_N(\omega) = \mathrm{i}[Z_c(\omega)/\varphi_0]\cot[k_c(\omega)L], \tag{8}$$

where φ_0 is the porosity, L is the thickness of the porous layer, and the characteristic impedance and the complex propagation constant are, respectively, defined as [33]

$$Z_c(\omega) = \sqrt{K(\omega)\rho(\omega)},$$

$$k_c(\omega) = \omega\sqrt{\rho(\omega)/K(\omega)} \tag{9}$$

in which the complex effective density and the complex bulk modulus are given as [33]

$$\rho(\omega) = \alpha\rho_0\left\{1 - \frac{\sigma\varphi_0}{\mathrm{i}\omega\alpha\rho_0}\,G_{\mathrm{J}}(\omega)\right\},$$
$$K(\omega) = \gamma p_0\left[\gamma - (\gamma-1)\left(1 - \frac{\sigma'\varphi_0}{\mathrm{i}Pr^2\omega\rho_0\alpha}\,G'_{\mathrm{J}}(Pr^2\omega)\right)^{-1}\right]^{-1}, \tag{10}$$

where α and σ are tortuosity and flow resistivity of the porous material, p_0 is the ambient pressure, and $G_{\mathrm{J}}(\omega)$ and $G'_{\mathrm{J}}(\omega)$ are the dynamic viscosity and thermal correction factors which are written as [33]

$$G_{\mathrm{J}}(\omega) = \left\{1 - \mathrm{i}\frac{4\alpha^2\eta\rho_0\omega}{\sigma^2\Lambda^2\varphi_0^2}\right\}^{1/2},$$
$$G'_{\mathrm{J}}(Pr^2\omega) = \left\{1 - \mathrm{i}\frac{4\alpha^2\eta\rho_0\omega Pr^2}{\sigma'^2\Lambda'^2\varphi_0^2}\right\}^{1/2} \tag{11}$$

in which the viscous and thermal characteristic lengths are, respectively, determined from $\Lambda \approx \sqrt{8\alpha\eta/\varphi_0\sigma}/c$, $\Lambda' \approx \sqrt{8\alpha\eta/\varphi_0\sigma}/c'$, where c is a shape factor whose order of magnitude lies between 0.3 and 3.0 for most materials, $c' = \sqrt{\sigma'/\sigma}$ is a coefficient that is smaller or equal to c.

The unknown modal coefficients $a_n(\omega)$ and $b_n(\omega)$, which are explicitly present in Eqs. (5) and (6), must be determined by the application of suitable boundary conditions. Accordingly, the continuity of normal velocity at the surface of each cylinder requires

$$-\frac{\partial\Phi(r,\theta,\omega)}{\partial r}\bigg]_{r=\mathrm{a}} = \sum_{n=-\infty}^{\infty} u_n(\omega)\mathrm{e}^{\mathrm{i}n\theta},$$
$$-\frac{\partial\Phi(r^*,\theta^*,\omega)}{\partial r^*}\bigg]_{r^*=\mathrm{a}} = \sum_{n=-\infty}^{\infty} u_n^*(\omega)\mathrm{e}^{\mathrm{i}n\theta^*}, \tag{12}$$

where $u_n(\omega)$ and $u_n^*(\omega)$ represent the modal radial surface velocity amplitudes of the real and image cylinders, respectively. Next, incorporating the translational addition theorem 4 into boundary conditions (12) and utilizing the orthogonality of the transcendental harmonics yields

$$u_n(\omega) = -k\mathrm{H}'_n(ka)a_n(\omega) - Rk\mathrm{J}'_n(ka)\sum_{m=-\infty}^{\infty}\mathrm{H}_{n-m}(kd)b_m(\omega),$$
$$u_n^*(\omega) = -Rk\mathrm{J}'_n(ka)\sum_{m=-\infty}^{\infty}\mathrm{H}_{m-n}(kd)a_m(\omega) - k\mathrm{H}'_n(ka)b_n(\omega). \tag{13}$$

Now, following the analysis presented in [29, pp. 370–375] for inclusion of the boundary impedance effects on radiation load of a multipole source, the real and the image sources are taken to be of equal strength. Accordingly, as with the rigid boundary case, $u_n^*(\omega) = (-1)^n u_n(\omega)$ in Eq. (13), which leads to the following significant result: $b_n(\omega) = (-1)^n a_n(\omega)$ [28]. Consequently,

the expression for modal surface velocities of the real cylinder is conveniently reduced to

$$u_n(\omega) = -k\mathrm{H}_n'(ka)a_n(\omega) - Rk\mathrm{J}_n'(ka)\sum_{m=-\infty}^{\infty}(-1)^m a_m(\omega)\mathrm{H}_{n-m}(kd)$$
$$(n = \ldots, -3, -2, -1, 0, 1, 2, 3, \ldots). \tag{14}$$

Similarly, Fourier components of the surface pressure of the real cylinder is written as

$$p_n(\omega) = -\mathrm{i}\omega\rho_0\mathrm{H}_n(ka)a_n(\omega) - \mathrm{i}\omega\rho_0 R\mathrm{J}_n(ka)\sum_{m=-\infty}^{\infty}(-1)^m a_m(\omega)\mathrm{H}_{n-m}(kd)$$
$$(n = \ldots, -3, -2, -1, 0, 1, 2, 3, \ldots). \tag{15}$$

The fluctuating acoustic pressure on the surface of the vibrating cylinder constitutes its radiation loading. The radiation loading on the cylindrical surface excited in vibrational modes of various order (i.e., monopole, dipole, quadrupole, and other multipole-like radiators), as described through an acoustic radiation impedance matrix, is determined in two simple steps as follows. First, the truncated $(2N + 1) \times (2N + 1)$ systems of Eqs. (14) and (15) are advantageously put in the matrix form

$$\mathbf{u}(\omega) = \mathbf{R}(ka, kd, R)\mathbf{c}(\omega), \tag{16}$$

$$\mathbf{p}(\omega) = \mathbf{S}(ka, kd, R)\mathbf{c}(\omega), \tag{17}$$

where

$$\mathbf{u}(\omega) = [u_{-N}, \ldots, u_{-2}, u_{-1}, u_0, u_1, u_2, \ldots, u_N]^{\mathrm{T}},$$
$$\mathbf{c}(\omega) = [a_{-N}, \ldots, a_{-2}, a_{-1}, a_0, a_1, a_2, \ldots, a_N]^{\mathrm{T}},$$
$$\mathbf{p}(\omega) = [p_{-N}, \ldots, p_{-2}, p_{-1}, p_0, p_1, p_2, \ldots, p_N]^{\mathrm{T}}. \tag{18}$$

Next, incorporating Eq. (16) into Eq. (17), the column vector containing the modal surface pressures can conveniently be expressed in terms of modal surface velocities as

$$\mathbf{p}(\omega) = \mathbf{Z}(ka, kd, R)\mathbf{u}(\omega), \tag{19}$$

where the modal specific acoustic impedance matrix $\mathbf{Z}(ka, kd, R)$ is given by

$$\mathbf{Z}(ka, kd, R) = \mathbf{S}(ka, kd, R)\mathbf{R}^{-1}(ka, kd, R). \tag{20}$$

Here it can be noted that each element of the above fully populated impedance matrix may beneficially be put in terms of a resistive and a reactive component as [34]

$$z_{nm}(ka, kd, R) = r_{nm}(ka, kd, R) - \mathrm{i}x_{nm}(ka, kd, R). \tag{21}$$

3. Numerical results

In order to illustrate the nature and general behaviour of solution, a number of specific numerical examples are considered in this section. The ambient fluid is assumed to be air at atmospheric pressure and room temperature. To comply with the local surface reaction model, the absorbing surface material was selected to be a layer of (rigidly backed) "Domisol Coffrage" glass

Table 1
Input parameter values used in calculations

Parameter	Numerical value
p_0 (Pa)	1.00×10^5
$T(^\circ\mathrm{K})$	300.00
c_0 (m/s)	346.2
ρ_0 (kg/m^3)	1.18
η (kg/m s)	1.83×10^{-5}
η_b (kg/m s)	1.10×10^{-5}
γ	1.40
Pr	0.70
a (m)	0.10
L (m)	0.10
φ_0	0.94
α	1.06
σ (N m^{-4} s)	4.00×10^4
σ' (N m^{-4} s)	1.32×10^4
c	1.15

wool (manufactured by St. Gobain-Isover, Rantigny France). The numerical values for the physical properties of the medium, which are used in the calculations, are summarized in Table 1 [33]. Accurate computation of Bessel functions is achieved by employing MATLAB specialized math functions ''besselh'' and ''besselj''. Subsequently, a MATLAB code was constructed for treating boundary conditions, to determine the unknown modal coefficients, and to compute the modal impedance matrix, $\mathbf{Z} = \mathbf{S}\mathbf{R}^{-1}$, as functions of non-dimensional frequencies $ka = \omega a/c_0$ and $kd = \omega d/c_0$. Accurate computations for derivatives of cylindrical Bessel functions were accomplished by utilizing (9.1.27) in Ref. [31]. The computations were performed in double precision on a Pentium IV personal computer with a truncation constant of $N = 30$ to assure convergence in the high-frequency range, and also in case of close proximity of the source to the wall.

Before presenting the numerical results, the terminology used in the calculations has to be made clear in order to avoid possible confusion. In particular, by the term ''pulsating cylindrical surface'' or just ''pulsating cylinder'' refers to a cylindrical surface of radius ''a'' vibrating in the $n = 0$ (monopole-like or breathing or expanding) mode. Similarly, the term ''transversely oscillating cylinder'' or just ''oscillating cylinder'' denotes a cylindrical surface of radius ''a'' vibrating in the $n = 1$ (dipole-like or rigid body or shaking) mode. Furthermore, the term ''monopole (dipole) line source'' implies an array of point monopole (dipole) sources (i.e., no size/radius is involved). Figs. 2 and 3 show the resistive and the reactive components of radiation load on the pulsating and transversely oscillating cylinders, positioned near the impedance boundary of the acoustic halfspace as a function of the non-dimensional frequency kd at selected non-dimensional acoustic frequencies ($ka = 0.1, 1, 2, 3, 4$) and basic medium properties as given in Table 1. Also shown are the modal impedance components for the cylindrical surface located near a very high impedance (nearly rigid) surface. Thus, the computations are made for a very low (high) porosity (tortuosity) layer of (dense) porous material with following assumptions for its

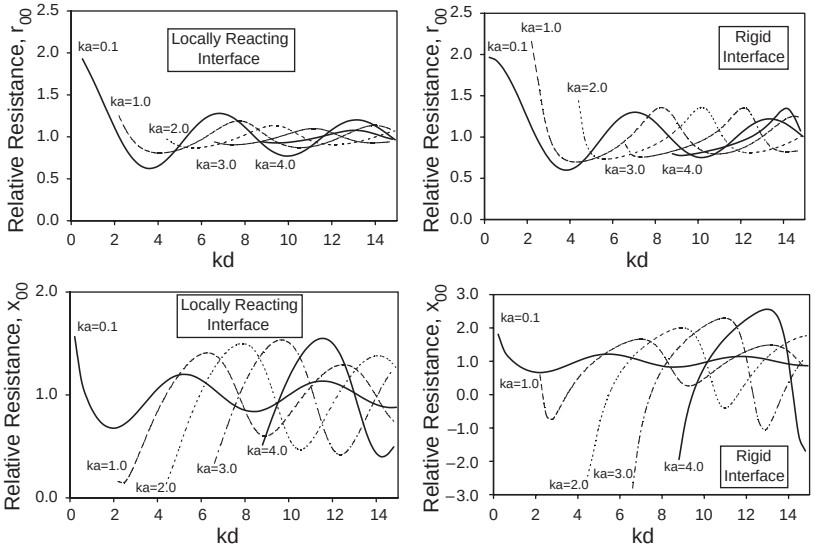

Fig. 2. Resistive and reactive components of modal acoustic impedance load on a pulsating cylinder positioned near the halfspace boundary as a function of the distance parameter *kd* at selected nondimensional frequencies.

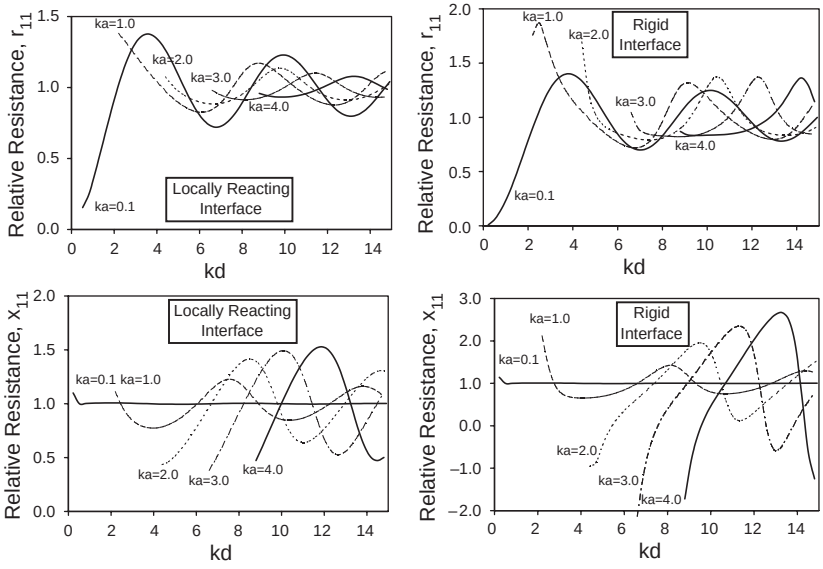

Fig. 3. Resistive and reactive components of modal acoustic impedance load on a transversely oscillating cylinder positioned near the halfspace boundary as a function of the distance parameter *kd* at selected nondimensional frequencies.

physical property values: $\varphi_0 = 0.001$, $\alpha = 31.62$, $\sigma = 9 \times 10^6$ (N m^{-4} s), and $\sigma' = 1 \times 10^6$ (N m^{-4} s). Furthermore, in order to make clear evaluations, all modal impedance values are divided by the corresponding infinite medium radiation components. Comparison of the figures leads to the following observations. First, as the non-dimensional frequency is increased,

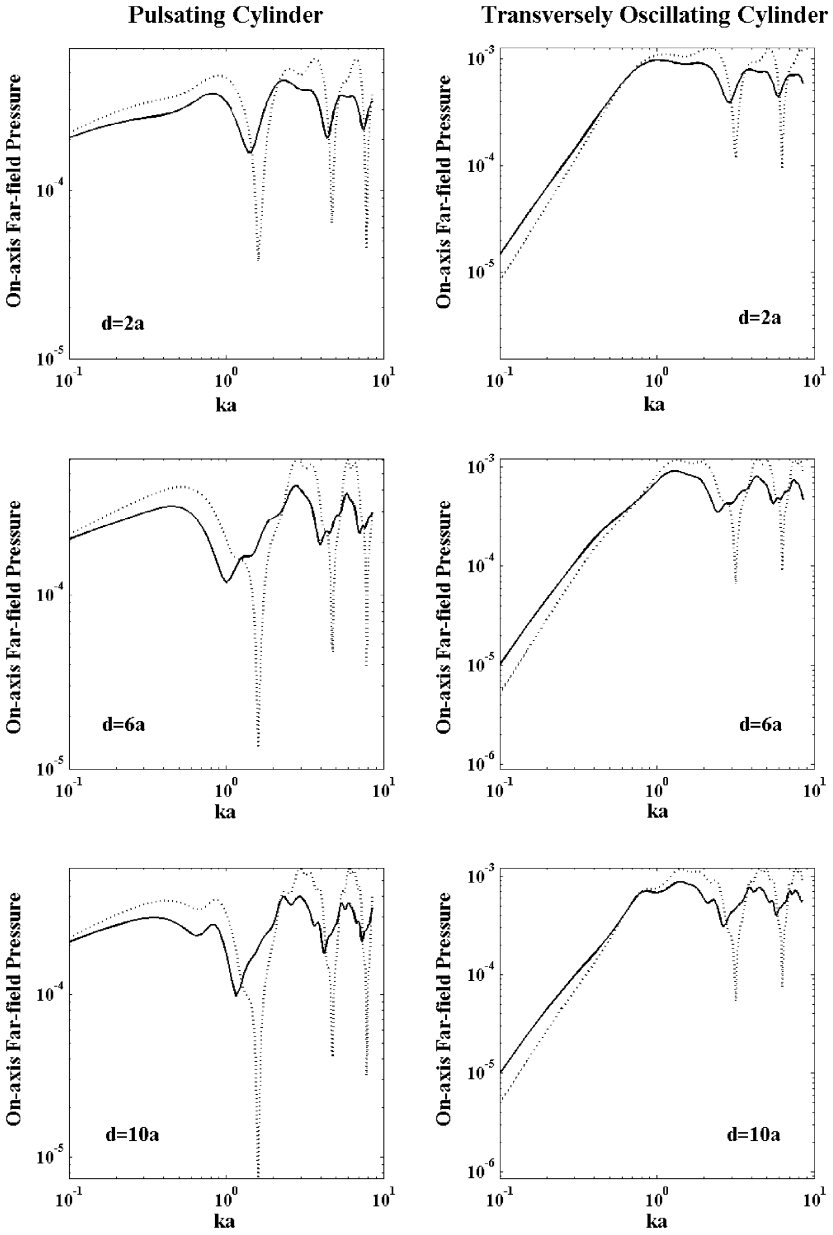

Fig. 4. Variation of the on-axis farfield acoustic pressure with radiation frequency ka at the selected distance parameters [solid lines: locally reacting boundary, dashed lines: rigid wall; the pressure magnitudes are normalized by $\rho_0 c_0^2$].

all modal resistance (reactance) values approach the free field value of unity (zero) in an oscillatory manner. Second, markedly smaller modal impedance component magnitudes in the locally reacting boundary case are observed in comparison to the "rigid" wall situation, especially at the intermediate and higher frequencies ($ka \geqslant 1$). In addition, relatively milder oscillations in the modal impedance curves for the source near the passive wall are seen in all figures. Moreover, in the "rigid" interface case, a negative modal reactance is detected (i.e., the reactance becomes predominantly stiffness controlled in these regions [34]) for a relatively wide range of frequencies as compared to the locally reacting example.

Fig. 4 displays the change in the on-axis radiated far-field acoustic pressure (i.e., $\lim_{r\to\infty}|p(r,\theta=0,\omega)|/\rho_0 c_0^2$) with the excitation frequency at the selected distance parameters. The farfield value of the radial coordinate in each case is numerically determined by making several computer runs with increasing radial co-ordinates while looking for a fixed radiated farfield pressure directivity pattern. The choice of $r_\infty = 100a$ is computed to be adequate in all cases. It is informative to study the change in the on-axis radiated far-field pressure as the source excitation frequency and position are varied. The main effect of the presence of the locally reacting boundary (solid lines) in comparison with the rigid wall case (dashed lines) is the widespread disappearance of sharp dips from the radiated pressure curves. Furthermore, a general reduction in pressure magnitudes, especially for the pulsating cylinder located not very close to the boundary, is observed. There is also a relatively wide variation of the pressure magnitudes in the transversely oscillating cylinder case in comparison with the pulsating cylinder situation. The primary effect of increasing the distance parameter is to superimpose small oscillations and increase the overall sharpness of the pressure curves. Last but not least, the most surprising

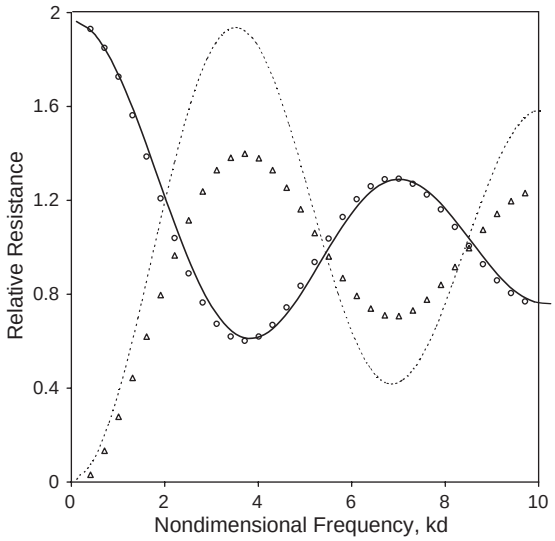

Fig. 5. Comparison of the relative radiation resistance of a very small sized pulsating (transversely oscillating) cylindrical surface positioned near the locally reacting wall with that of a monopole (dipole) line source as a function of the distance parameter kd (— monopole line source; - - - dipole line source; ○ pulsating cylinder ($ka = 0.05$); △ oscillating cylinder ($ka = 0.05$)).

observation is the adverse effect of the locally reacting boundary on the radiated farfield pressure for the transversely oscillating cylinder in the low-frequency range.

Finally, in order to check overall validity of the work, the code for the case of a particularly small cylindrical surface vibrating near the locally reacting wall was first executed at a very low non-dimensional frequency ($ka = 0.05$). Fig. 5 compares the outcome with the corresponding line source results that are computed using Eqs. (A.1) and (A.9) in Appendix A. In order to make clear evaluations, all resistance values are divided by the corresponding infinite medium radiation components. Evidently, excellent agreement is obtained in the pulsating cylinder case. This is due to the fact that Eq. (A.1) is indeed an exact approximation for a pulsating cylindrical surface of small radius ($ka \ll 1$) [35]. On the other hand, the numerical comparison appears to be less good for the transversely oscillating cylinder as the physical nature and the mathematical representation used for a dipole line source are entirely different from that of the oscillating cylinder. This can readily be observed by (numerical) comparison of the general field radiated from a unit amplitude dipole line source (i.e., Eq. (A.6)) with that of a transversely oscillating cylindrical surface (i.e., $H_1(kr)\cos\theta$). Next, to further assess the accuracy of the work, the code was used to compute the total acoustic pressure ($|p(kX, kY)|$) due to unit pressure amplitude pulsation of a cylindrical surface of small radius ($ka \ll 1$) positioned very close to a constant impedance planar boundary ($kd \approx 0, \beta = 1 + 0.5\mathrm{i}$). Fig. 6 compares the results with that of geometric acoustic approximation for a simple (monopole) line source at an impedance boundary. The agreement is good in all points. The geometric acoustic plot (Fig. 6b) is generated using the following approximation [21]:

$$p(kX, kY) = H_0(kr) + \frac{\cos\theta' - \beta}{\cos\theta' + \beta} H_0(kr^*), \tag{22}$$

where $r, r^* = \sqrt{(X \mp d/2)^2 + Y^2}$ (see Fig. 1). Lastly, it is noted that all modal impedance results [i.e., $r_{00}(\omega), r_{11}(\omega), \ldots$] are simultaneously generated using a single code based on our impedance matrix formulation which increases the confidence in the computational technique and the computer code used for generating these results.

4. Conclusions

The modal acoustic radiation impedance load and the on-axis farfield radiated pressure have been computed for a cylindrical surface undergoing modal vibrations close to a finite impedance boundary. These results are the product of an exact treatment of the fluid/structure interaction that involves utilization of the appropriate wave field expansions and boundary conditions along with the method of images, translational addition theorems for cylindrical wave functions, and the proper description of dynamic permeability effects in the rigid-frame porous materials. It also incorporates a simple approximate analytical model describing the radiation of sound from the cylindrical surface located close to the locally reacting planar interface through a complex amplitude wave reflection coefficient. The numerical results display relatively smaller amplitudes and milder oscillations of the modal impedance components and the on-axis farfield radiated pressure for both modes of cylindrical surface vibrations near the locally reacting boundary in comparison to the "rigid" wall situation. Furthermore, the modal reactance values predominantly

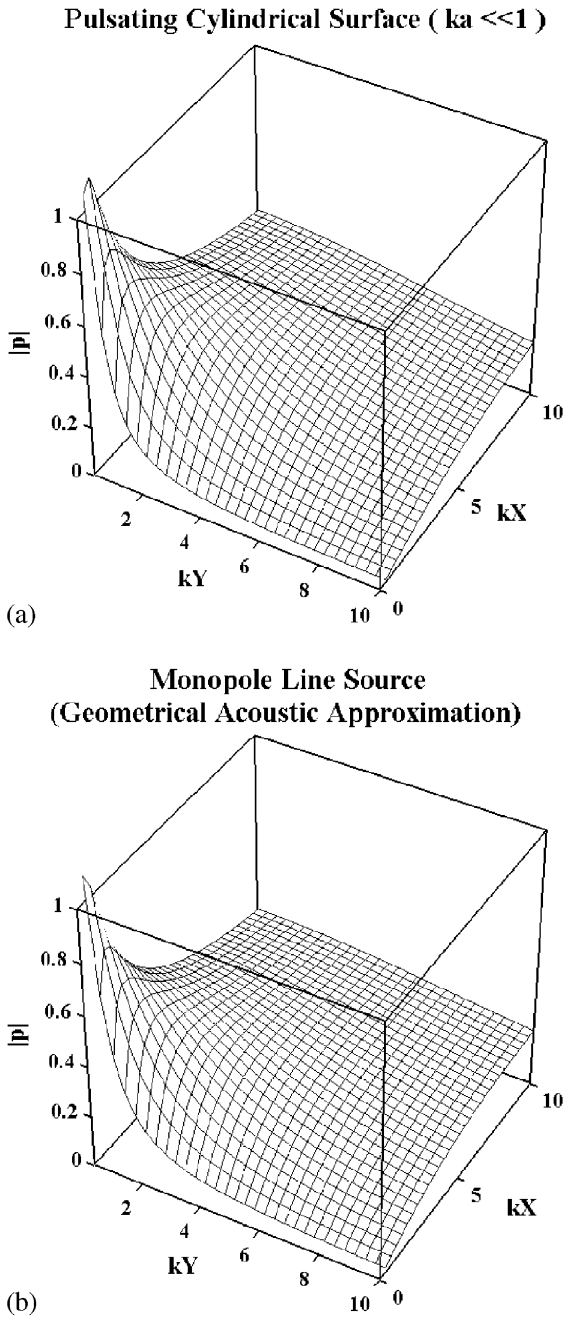

Fig. 6. Comparison of the total sound pressure field for (a) unit pressure amplitude pulsation of a cylindrical surface of small radius located very close to a constant impedance planar boundary ($kd \approx 0$, $\beta = 1 + 0.5\mathrm{i}$), with (b) geometric acoustic approximation of a simple (monopole) line source at the impedance boundary.

remain positive in the entire frequency range of interest, which is in direct contrast to the "rigid" interface (largely stiffness controlled) case. The most surprising behaviour is the adverse effect of the absorbing boundary condition on the radiated farfield pressure magnitudes for the transversely oscillating cylinder in the low-frequency range.

Acknowledgements

The author wishes to sincerely thank Professors K.B. Rusmussen, J.F. Allard, M.R. Stinson, J.S. Bolton, D.L. Johnson, and S. Taherzadeh for valuable and productive consultations on acoustic theory of porous media. They are also indebted to a demanding reviewer whose constructive critique lead to substantial improvement of the manuscript.

Appendix A. Radiation from a dipole line source over an impedance plane

First, following the lucid theoretical development by Morse and Ingard [29], the acoustic power radiated (per unit length) by a pulsating cylindrical source of small radius near an impedance plane can be proposed from that of two pulsating parallel cylindrical sources of small radii ($ka \ll 1$) as [35]

$$N = N_1^0[1 + R\mathrm{J}_0(kd)], \tag{A.1}$$

where N_1^0 is the power generated by a single source, J_0 is cylindrical Bessel function of zero order [31], and d is the distance between the real and image sources.

Next, it is intended to derive the appropriate expressions for a vertical dipole line source near an impedance boundary. If a positive monopole line source and a negative sound source are brought close to each other, an acoustic dipole results. If r_+ is the distance of the field point from the

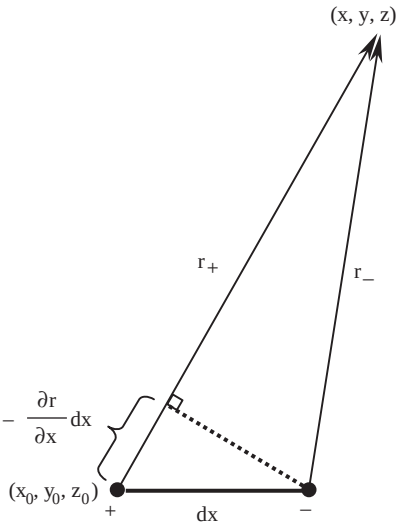

Fig. 7. Construction of an acoustic dipole from two monopole line sources.

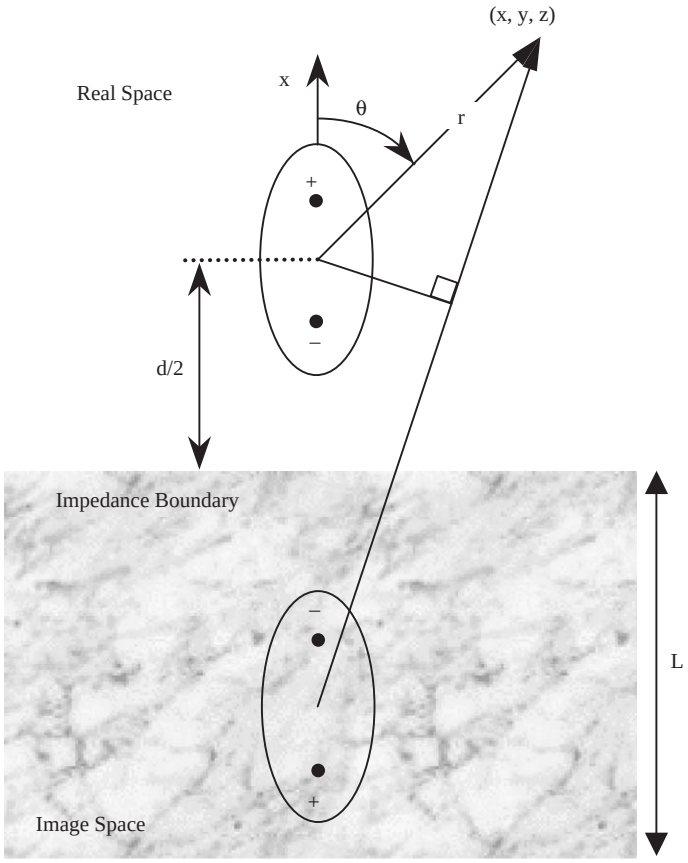

Fig. 8. Acoustic dipole line source near an impedance boundary.

positive source and r_- is the distance of the field point from the negative source, the resultant field becomes (Fig. 7)

$$p = A\left(\frac{\mathrm{e}^{-\mathrm{i}kr_+}}{\sqrt{kr_+}} - \frac{\mathrm{e}^{-\mathrm{i}kr_-}}{\sqrt{kr_-}}\right), \tag{A.2}$$

where p stands for the pressure or velocity potential. As the distance between the two sources decreases, the above difference can be expressed by a differential

$$p = A\frac{\partial}{\partial x_0}\left(\frac{\mathrm{e}^{-\mathrm{i}kr}}{\sqrt{kr}}\right)\mathrm{d}x = A\frac{\partial}{\partial r}\left(\frac{\mathrm{e}^{-\mathrm{i}kr}}{\sqrt{kr}}\right)\frac{\partial r}{\partial x_0}\,\mathrm{d}x, \tag{A.3}$$

where (x_0, y_0, z_0) are the coordinates of the source position and (x, y, z) are those of the field point. Now, employing cartesian co-ordinates

$$r = \sqrt{(x - x_0)^2 + (y - y_0)^2 + (z - z_0)^2}, \tag{A.4}$$

gives

$$\frac{\partial r}{\partial x} = -\frac{\partial r}{\partial x_0} = \cos\theta. \tag{A.5}$$

Hence (A.3) becomes

$$p = \frac{A^*}{\sqrt{kr}}\left(1 + \frac{1}{2\mathrm{i}kr}\right)\mathrm{e}^{-\mathrm{i}kr}\cos\theta \tag{A.6}$$

in which $A^* = -\mathrm{i}kA\,\mathrm{d}x$.

When a dipole line source is positioned a distance $d/2$ above an impedance wall, an image source is formed at a distance $d/2$ below the wall (Fig. 8). Hence, the resultant far-field sound pressure may be written as

$$p = A^*\left[\cos\theta\frac{\mathrm{e}^{-\mathrm{i}kr}}{\sqrt{kr}} + R\cos\theta\frac{\mathrm{e}^{-\mathrm{i}k(r+d\cos\theta)}}{\sqrt{k(r+d\cos\theta)}}\right]. \tag{A.7}$$

Next, assuming r to be large, the term "$d\cos\theta$" can be neglected in the denominator, and thus

$$p = A^*\cos\theta\frac{\mathrm{e}^{-\mathrm{i}k(r+\frac{d}{2}\cos\theta)}}{\sqrt{kr}}\left(\mathrm{e}^{(\mathrm{i}kd/2)\cos\theta} + R\mathrm{e}^{-(\mathrm{i}kd/2)\cos\theta}\right). \tag{A.8}$$

Finally, the total radiated sound power (per unit source length) can be determined by substituting the above expression into [35]

$$N = \int \frac{p^2}{2\rho_0 c_0}\,\mathrm{d}A, \tag{A.9}$$

where the above integral may readily be evaluated by numerical integration.

References

[1] L.L. Beranek, Acoustical properties of homogeneous, isotropic rigid tiles and flexible blankets, *Journal of the Acoustical Society of America* 19 (1947) 556–568.
[2] C. Zwikker, C.W. Kosten, *Sound Absorbing Materials*, Elsevier, Amsterdam, 1949.
[3] F. Gassmann, Über die Elastizität poroser Medien, *Vierteljahrsschrift der Naturforschenden Gesellschaft in Zürich* 96 (1951) 1–23.
[4] M.A. Biot, Theory of propagation of elastic waves in a fluid-saturated porous solid, I: low-frequency range, *Journal of the Acoustical Society of America* 28 (1956) 168–178.
[5] M.A. Biot, Theory of propagation of elastic waves in a fluid-saturated porous solid, II: higher frequency range, *Journal of the Acoustical Society of America* 28 (1956) 179–191.
[6] M.A. Biot, Mechanics of deformation and acoustic propagation in porous media, *Journal of Applied Physics* 23 (1962) 1482–1498.
[7] T.J. Plona, Observation of the second compressional wave in a porous medium at ultrasonic frequencies, *Applied Physics Letter* 36 (1980) 259–261.
[8] J.G. Berryman, Confirmation of Biot's theory, *Applied Physics Letter* 73 (1980) 382–384.
[9] B. Gurevich, O. Kelder, D.M.J. Smeulders, Validation of the slow compressional wave in porous media: comparison of experiments and numerical simulations, *Transport in Porous Media* 36 (1999) 149–160.
[10] I. Rudnick, The propagation of an acoustic wave along a boundary, *Journal of the Acoustical Society of America* 19 (1947) 348–356.

[11] A. Sommerfeld, Uber die ausbreitung der wellen in der drahtlosen telegraphie, *Annals of Physics* 28 (1909) 665–736.
[12] M.R. Stinson, A note on the use of an approximate formula to predict sound fields above an impedance plane due to a point source, *Journal of the Acoustical Society of America* 98 (1995) 1810–1812.
[13] F.X. Becot, Oriented study of the tyre/road noise including the ground effects, Chalmers University of Technology, Sweden, Report F 01-05, 2001.
[14] W. Kropp, F.X. Becot, S. Barrelet, On the sound radiation from tyres, *Acta Acustica united with Acustica* 86 (2000) 769–779.
[15] D. Ouis, Noise shielding by simple barriers: comparison between the performance of spherical and line sound sources, *Journal of Computational Acoustics* 8 (2000) 495–502.
[16] G.R. Watts, Traffic noise barriers, *TRL Annual Review* (Online), 1995, available: http://www.trl.co.uk.
[17] D. Habault, P. Filippi, Diffraction d'une onde cylindrique monochromatique par differents modeles de sols plans, *Acustica* 46 (1980) 1–7.
[18] S.N. Chandler-Wilde, D.C. Hothersall, Sound propagation above an inhomogeneous plane, *Journal of Sound and Vibration* 98 (1985) 475–491.
[19] K.B. Rasmussen, Line source propagation over an impedance surface, Acoustic Laboratory Technical University, Denmark, Report 58, 1994.
[20] C.F. Chien, W.W. Soroka, A note on the calculation of sound propagation along an impedance surface, *Journal of Sound and Vibration* 69 (1980) 340–343.
[21] F.P. Mechel, A line source above a plane absorber, *Acta Acustica united with Acustica* 86 (2000) 203–215.
[22] A.V. Generalov, Sound field of a multipole source of order N near a locally reacting surface, *Soviet Physics Acoustics* 33 (1987) 492–495.
[23] K.M. Li, S. Taherzadeh, K. Attenborough, Sound propagation from a dipole source near an impedance plane, *Journal of the Acoustical Society of America* 101 (1997) 3343–3352.
[24] K.M. Li, S. Taherzadeh, The sound field of an arbitrarily oriented quadrupole near ground surface, *Journal of the Acoustical Society of America* 102 (1997) 2050–2057.
[25] Z. Hu, J.S. Bolton, Sound propagation from an arbitrary oriented multipole placed near a plane, finite impedance surface, *Journal of Sound and Vibration* 170 (1994) 637–699.
[26] S.M. Hasheminejad, H. Hosseini, Radiation loading of a cylindrical source in a fluid-filled cylindrical cavity embedded within a fluid-saturated poroelastic medium, *Journal of Applied Mechanics* 69 (2002) 675–683.
[27] S.M. Hasheminejad, Modal impedances for a spherical source in a fluid-filled spherical cavity embedded within a fluid-infiltrated elastic porous medium, *International Journal of Solids and Structures* 35 (1998) 129–148.
[28] S.M. Hasheminejad, Modal acoustic on a spherical radiator in an acoustic halfspace with locally reacting boundary, *Acta Acustica united with Acustica* 87 (2001) 443–453.
[29] P.M. Morse, K.U. Ingard, *Theoretical Acoustics*, McGraw-Hill, New York, 1968.
[30] A.D. Pierce, *Acoustics: An Introduction to its Physical Principles and Applications*, McGraw-Hill, New York, 1981.
[31] M. Abramovitz, I.A. Stegan, *Handbook of Mathematical Functions*, National Bureau of Standards, Washington, DC, 1964.
[32] Y.A. Ivanov, Diffraction of Electromagnetic Waves on Two Bodies, NASA Technical Trans. F-597, 1970.
[33] J.F. Allard, *Propagation of Sound in Porous Media*, *Modelling Sound Absorbing Materials*, Elsevier Applied Science, London, 1993.
[34] M.C. Junger, D. Feit, *Sound, Structures, and Their Interaction*, MIT Press, Cambridge, MA, 1972.
[35] E. Skudrzyk, *The Foundations of Acoustics*, Springer, New York, 1971, pp. 445–446.